inter.noise
HAMBURG 2016

Efficient edge source approach to the modeling of multi-edge noise barrier tops

U. Peter SVENSSON[1]; Sara R. MARTIN[1,2]; Andreas ASHEIM[3]

[1]Acoustics Research Centre, Department of Electronics and Telecommunications, NTNU, Norwegian University of Science and Technology, Trondheim, Norway

[2]Presently at CCRMA, Stanford University, CA, USA

[3]Department of Mathematical Sciences, NTNU, Norwegian University of Science and Technology, Trondheim, Norway

ABSTRACT

The scattering from rigid polyhedra can be efficiently and accurately modelled with an edge source integral equation. The modeling is based on a separation of the sound field into three terms: a geometrical-acoustics term, a term which represents first-order diffraction, and a term which represents second- and higher-order diffraction. It is the latter term which is expressed through an integral equation whereas the first two terms are available explicitly. One set of noise barrier designs, infinite barriers with parallel-edge top designs, can furthermore be modelled with a particularly efficient form of that integral equation which exploits the symmetry property of the parallel edges and plane wave incidence. The symmetry formulation will be demonstrated in this paper, together with numerical examples and a discussion of implementation issues. Special numerical issues are related to singularities in certain scattering directions, and to the computation of the oscillating integrals that result. The underlying integral equation is valid for convex scatterer geometries, and the issues with non-convex geometries will furthermore be discussed together with examples such as Y-shaped noise barrier top designs.

Keywords: Noise barrier, Diffraction I-INCE Classification of Subjects Number(s): 23.4, 31.1

1 INTRODUCTION

The modeling of noise barriers is a well-researched field, where many different approaches have been used. For infinite barriers, the semi-empirical Maekawa charts[1] are very practical and have been used frequently. Numerical approaches for infinite barriers include those based on the Kirchhoff diffraction approximation (Fresnel-zone based)[2], or the Geometrical Theory of Diffraction (GTD)[2]. Accurate predictions, of infinite- or finite-length barriers can be done with the boundary element method[3], the finite element method or finite differences schemes. As shown by Duhamel, a 2D-calculation can be transformed into a 2.5D case, that is, convert a line-source to a point-source ensonification, for an infinite noise barrier[4].

Another category of methods is based on edge-diffraction modeling. A building block for those methods is the infinite rigid-walled wedge, with exact solutions in the frequency domain[5] and time domain[6]. More realistic models of noise barriers than single-edge wedges need to take the thickness into account. An exact solution has been presented for the truncated wedge, which includes the thick noise barrier case[7]. Multiple-edge prisms, or polygonal cylinders, have been modeled with the high-frequency asymptotic Uniform Theory of Diffraction[8]. These diffraction-based methods have all considered infinite edges, but finite-length edges, that form polyhedra, were studied by Medwin et al[9], also for two-edge cases. The Biot-Tolstoy and Medwin approaches were further extended into time-domain[10] and frequency-domain[11] solutions that were taking higher orders of diffraction into account via a computationally costly iterative approach. Finally, an edge-

source integral equation formulation (ESIE) in the frequency-domain[12] and the time-domain[13] permitted the efficient computation of scattering/diffraction from convex, rigid-walled polyhedra up to arbitrarily high orders of diffraction. Results were demonstrated to be accurate down to 0 Hz, which was noteworthy considering that the diffraction waves are added to a classical geometrical-acoustics solution, a high-frequency asymptotic solution. These latter ESIE-based methods can handle arbitrary finite and semi-infinite 3D scattering polyhedra. However, the typical geometry of a noise barrier has a long extension in one dimension, which leads to large computational challenges, also for the efficient ESIE-based methods. Therefore, the purpose of this paper is to derive an ESIE formulation which is valid for infinitely long noise barriers with multiple edges, and plane- or cylindrical wave incidence.

In section 2, the general 3D-formulation ESIE-formulation[12], is rewritten into a form valid for the special noise barrier case, with computational aspects discussed in section 3, and some example results are presented in section 4.

2 THEORY

The sound field around a noise barrier is viewed as the solution to the scattering problem for a convex polyhedron of n_E edges, decomposed into geometrical acoustics components (direct sound and specular reflections), first-order diffraction, and higher-order diffraction. The sound pressure at a receiver position, $\mathbf{r}$, is

$$p(\mathbf{r}) = p_{\text{direct}} + p_{\text{specular}} + \sum_{i=1}^{n_E} p_{\text{diffr. 1,edge } i} + \sum_{i=1}^{n_{\max,order2}} p_{\text{diffr.2, edge-to-edge combination } i} + \cdots$$

$$= p_{\text{direct}} + p_{\text{specular}} + \sum_{i=1}^{n_E} p_{\text{diffr. 1,edge } i} + p_{\text{HOD}} \tag{1}$$

where $p_{\text{diffr. 1,edge } i}$ represents an edge diffraction wave from the source, $\mathbf{r}_\text{S}$, via edge i, to the receiver, $\mathbf{r}$. Furthermore, $p_{\text{diffr.2, edge-to-edge combination } i}$ represents a second-order diffraction wave, from the source, via two edges, and then to the receiver, etc. The number of second-,third- and higher-order diffraction waves grows with a rate which depends on the geometry of the polyhedron. All second- and higher-order diffraction terms are contained in the term p_{HOD}.

It should be noted that all the terms in Eq. 1. are subject to visibility factors, $V_{\mathbf{r}_2,\mathbf{r}_1}$, which take the value 0 or 1, depending on whether the geometrical path from the point $\mathbf{r}_1$ to $\mathbf{r}_2$ is obstructed or not. As one example, a receiver behind a noise barrier can not see a source on the other side of the barrier and thus the corresponding visibility factor, $V_{\mathbf{r},\mathbf{r}_\text{S}}$, is 0. As another example, a first-order diffraction wave via edge i, is valid only if both the source and the receiver can see the edge, that is, if $V_{\text{e}_\text{i},\mathbf{r}_\text{S}} \cdot V_{\mathbf{r},\text{e}_\text{i}} = 1$.

The terms p_{direct} and p_{specular} in Eq. 1 are directly available via, e.g., the image source method. The third term in Eq. 1 can be computed via the explicit line integrals that were presented by Svensson et al,[11], using, e.g., the numerical method of steepest descent as shown by Asheim and Svensson[14]. The computation of the higher-order diffraction terms, from order two and up, is done via the introduction of secondary edge sources that are placed along the edges. Each such source, placed in position z_1 along one edge, will have an amplitude $q(z_2, z_1)$ which represents the diffracted sound pressure in the direction of a position z_2 along another edge. Consequently, these edge sources can be viewed as directional sources, the directivity of which is specified not in terms of radiation/diffraction exit angle, but rather as function of the edge source position that will be hit by a diffracted wave. The values of these edge source signals, q, can be found via an integral equation, as described in section 2.1, and once the integral equation has been solved, the edge source signals represent all second- and higher-order diffraction. The edge source signals are, subsequently, propagated to give the sound pressure in a receiver position, and this propagation is presented in section 2.3.

This two-stage approach has many similarities with the boundary element method, with the important difference that here, only the edges, rather than the surfaces, of the scattering object

must be discretized in order to solve the integral equation. Another difference is that the boundary element method has numerical problems at certain frequencies due to internal fictive resonances for external scattering problems, whereas the edge source approach has no such problems. On the other hand, the edge-source based methods have numerical challenges in certain receiver positions, as discussed further in section 3.2.

In the next section, the special case of a convex, polygonal cylinder of infinite length will be studied.

2.1 Diffraction from a convex polygonal cylinder

Consider a convex polygonal cylinder as in Figure 1, with n_{E} edges, of either a "closed cylinder", Figure 1a, or "open cylinder", Figure 1b, geometry. The position along edge number i, e_i, is denoted by z_i. We will study edge source signals, $q^+_{e_i}(z_{i+1}, z_i)$ and $q^-_{e_i}(z_{i-1}, z_i)$, which are the source signals of edge sources located at position z_i of edge e_i, radiating either in the direction of edge e_{i+1}, position z_{i+1}, or in the direction of edge e_{i-1}, position z_{i-1}, respectively. It can be noticed that the diffraction wave from one edge can reach only those two closest neighbouring edges because of the convex shape of the polygonal cylinders which are studied here.

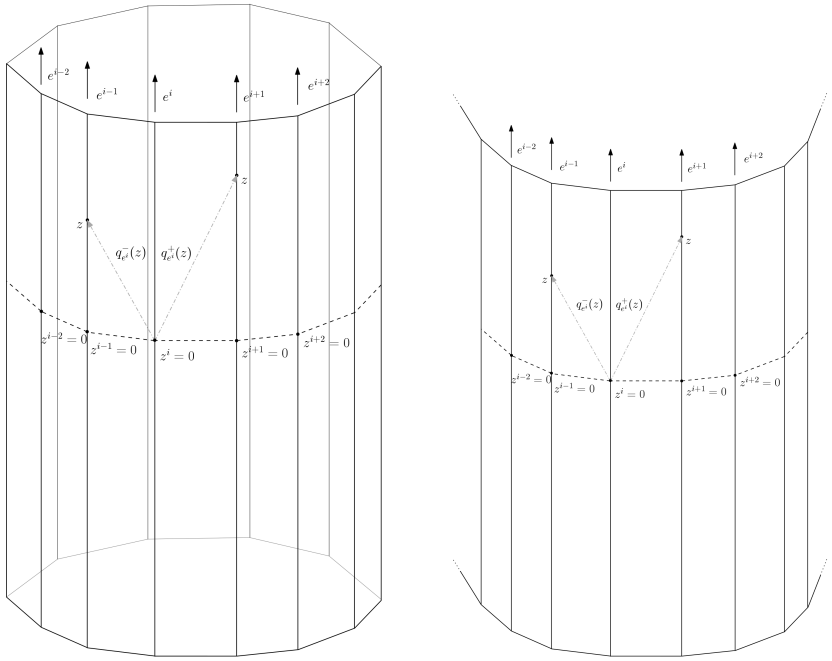

(a) (b)

Figure 1 – Illustration of a convex polygonal cylinder of type (a) closed cylinder, or (b) open cylinder. The open cylinder type could represent a noise barrier with a rounded top.

2.2 The integral equation for the edge source signal

The edge source signal $q^+_{e_i}(z_{i+1}, z_i)$ is given by re-diffraction of the contributions from the two closest neighbour edges, plus the contribution from the primary source, which is denoted $q^+_{e_i,0}(z_{i+1}, z_i)$,

$$q^+_{e_i}(z_{i+1}, z_i) = q^+_{e_i,0}(z_{i+1}, z_i) - \frac{\nu_i}{4\pi} \int_{-\infty}^{\infty} \frac{\mathrm{e}^{-\mathrm{j}kr_{z_i,z_{i-1}}}}{r_{z_i,z_{i-1}}} \beta_{e_{i+1},e_i,e_{i-1}}(z_{i+1}, z_i, z_{i-1}) q^+_{e_{i-1}}(z_i, z_{i-1}) dz_{i-1}$$

$$-\frac{\nu_i}{4\pi}\int_{-\infty}^{\infty}\frac{\mathrm{e}^{-\mathrm{j}kr_{z_i,z_{i+1}}}}{r_{z_i,z_{i+1}}}\beta_{e_{i+1},e_i,e_{i+1}}(z_{i+1},z_i,z_{i+1})q^-_{e_{i+1}}(z_i,z_{i+1})dz_{i+1} \tag{2}$$

where the directivity function is denoted $\beta_{e_{i+1},e_i,e_{i-1}}(z_{i+1},z_i,z_{i-1})$ to indicate that it represents the diffraction from position z_{i-1} on edge e_{i-1}, via position z_i on edge e_i, in the direction of position z_{i+1} on edge e_{i+1}. Furthermore, $r_{z_i,z_{i+1}}$ is the distance between the two edge points z_i and z_{i+1}, and ν_i is the so-called wedge index of edge number i, which is determined by the wedge angle of edge i. More details on the notation are given by Asheim and Svensson[12]. The contribution from the primary source is given by

$$q^+_{e_i,0}(z_{i+1},z_i) = -\frac{1}{4\pi}\nu_i V_{z_{i+1},z_i}V_{z_i,S}\frac{\mathrm{e}^{-\mathrm{j}kr_{z_i,S}}}{r_{z_i,S}}\beta(z_{i+1},z_i,S) \tag{3}$$

We will now consider the situation where the external source is either very far away, or a line source which is parallel to the infinite edges. Then the edge source signals must be identical along the edges such that

$$q^+_{e_i}(z_{i+1},z_i) = q^+_{e_i}(z_{i+1}+\Delta z, z_i+\Delta z) \qquad \forall \Delta z\in\mathbb{R} \tag{4}$$

and likewise for $q^-_{e_i}(z_{i-1},z_i)$. In particular, Eq. (4) holds for $\Delta z = -z_i$, such that

$$q^\pm_{e_i}(z_{i\pm1},z_i) = q^\pm_{e_i}(z_{i\pm1}-z_i,0) \tag{5}$$

and we represent the source signal at any position z_i on the edge e_i in the direction of position $z_{i+1}\in e_{i+1}$ by compact edge source signals,

$$q^+_{e_i}(z) := q^+_{e_i}(z,0) = q^+_{e_i}(z_{i+1}-z_i,0) \qquad \text{and} \tag{6}$$

$$q^-_{e_i}(z) := q^-_{e_i}(z,0) = q^-_{e_i}(z_{i-1}-z_i,0) \tag{7}$$

Here we have abused the notation a bit by using the symbol q^+ both for the general function of two positions, $q^+_{e_i}(z_{i+1},z_i)$, and for the compact function of one position, $q^+_{e_i}(z)$. The integral equation for the edge source signal $q^+_{e_i}(z)$, for a position $z_i=0$, along edge e_i, radiating in the direction of position z along edge e_{i+1}, is then

$$\begin{aligned} q^+_{e_i}(z) = q^+_{e_i,0}(z) &- \frac{\nu_i}{4\pi}\int_{\infty}^{\infty}\frac{\mathrm{e}^{-\mathrm{j}kr^+_{e_{i-1}}(\xi)}}{r^+_{e_{i-1}}(\xi)}\beta_{e_{i+1},e_i,e_{i-1}}(z,0,\xi)q^+_{e_{i-1}}(-\xi)d\xi \\ &-\frac{\nu_i}{4\pi}\int_{\infty}^{\infty}\frac{\mathrm{e}^{-\mathrm{j}kr^-_{e_{i+1}}(\xi)}}{r^-_{e_{i+1}}(\xi)}\beta_{e_{i+1},e_i,e_{i+1}}(z,0,\xi)q^-_{e_{i+1}}(-\xi)d\xi \end{aligned}$$

where the distance $r^+_{e_{i-1}}(\xi)$ is the distance from the position ξ on edge e_{i-1} to the position 0 on edge e_i. That distance is quite straightforward to compute, if one knows the width, w, of the facet between edges e_{i-1} and e_i, $r=\sqrt{\xi^2+w^2}$.

Now, symmetry implies that $q^+_{e_i}(-z) = q^+_{e_i}(z)$, so the integration ranges can be halved, but the edge directivity function is not symmetrical, that is, $\beta_{e_{i+1},e_i,e_{i-1}}(z,0,-\xi) \neq \beta_{e_{i+1},e_i,e_{i-1}}(z,0,\xi)$. This is handled by including the two mirrored values of the directivity function,

$$\begin{aligned} q^+_{e_i}(z) = q^+_{e_i,0}(z) &- \frac{\nu_i}{4\pi}\int_{0}^{\infty}\frac{\mathrm{e}^{-\mathrm{j}kr^+_{e_{i-1}}(\xi)}}{r^+_{e_{i-1}}(\xi)}\left[\beta_{e_{i+1},e_i,e_{i-1}}(z,0,\xi)+\beta_{e_{i+1},e_i,e_{i-1}}(z,0,-\xi)\right]q^+_{e_{i-1}}(\xi)d\xi \\ &-\frac{\nu_i}{4\pi}\int_{0}^{\infty}\frac{\mathrm{e}^{-\mathrm{j}kr^-_{e_{i+1}}(\xi)}}{r^-_{e_{i+1}}(\xi)}\left[\beta_{e_{i+1},e_i,e_{i+1}}(z,0,\xi)+\beta_{e_{i+1},e_i,e_{i+1}}(z,0,-\xi)\right]q^-_{e_{i+1}}(\xi)d\xi \end{aligned} \tag{8}$$

There will be one such integral equation for each $q_{e_i}^{\pm}(z)$, that is, one or two integral equations per edge.

2.3 The propagation integral for the edge source signals

Once the edge source signals have been established by solving the coupled integral equations, Eq. 8, the higher-order diffracted sound pressure, $p_{\mathrm{HOD}}(\mathbf{r})$, in an external position, $\mathbf{r}$, can be found via a propagation integral, summing up contributions from all edge pairs, (e_i, e_j), such that the last edge in each edge pair, e_i, can reach the receiver. Whether or not an edge source contribution can reach the receiver is encoded through the visibility factor, $V_{\mathbf{r},z_{i+1}}$. As a first step, we return to the two-parameter source signal formulation $q_{e_i}^{+}(z_{i+1}, z_i)$,

$$p_{\mathrm{HOD}}(\mathbf{r}) = -\frac{1}{8\pi}\sum_{i=1}^{n_E-1}\int_{-\infty}^{+\infty}\int_{-\infty}^{+\infty} q_{e_i}^{+}(z_{i+1}, z_i)\nu_{i+1}V_{z_{i+1},\mathbf{r}}\frac{e^{-jkr_{\mathbf{r},z_{i+1}}}}{r_{\mathbf{r},z_{i+1}}}\frac{e^{-jkr_{z_{i+1},z_i}}}{r_{z_{i+1},z_i}}\beta_{\mathbf{r},e_{i+1},e_i}(\mathbf{r}, z_{i+1}, z_i)dz_i dz_{i+1}$$

$$-\frac{1}{8\pi}\sum_{i=2}^{n_E}\int_{-\infty}^{+\infty}\int_{-\infty}^{+\infty} q_{e_i}^{-}(z_{i-1}, z_i)\nu_{i-1}V_{z_{i-1},\mathbf{r}}\frac{e^{-jkr_{\mathbf{r},z_{i-1}}}}{r_{\mathbf{r},z_{i-1}}}\frac{e^{-jkr_{z_{i-1},z_i}}}{r_{z_{i-1},z_i}}\beta_{\mathbf{r},e_{i-1},e_i}(\mathbf{r}, z_{i-1}, z_i)dz_i dz_{i-1}$$

and replace the $q_{e_i}^{+}(z_{i+1}, z_i)$ with the compact formulation, $q_{e_i}^{+}(z) = q_{e_i}^{+}(z_{i+1} - z_i)$,

$$p_{\mathrm{HOD}}(\mathbf{r}) = -\frac{1}{8\pi}\sum_{i=1}^{n_E-1}\int_{-\infty}^{+\infty}\int_{-\infty}^{+\infty} q_{e_i}^{+}(z_{i+1}-z_i)\nu_{i+1}V_{z_{i+1},\mathbf{r}}\frac{e^{-jkr_{\mathbf{r},z_{i+1}}}}{r_{\mathbf{r},z_{i+1}}}\frac{e^{-jkr_{z_{i+1},z_i}}}{r_{z_{i+1},z_i}}\beta_{\mathbf{r},e_{i+1},e_i}(\mathbf{r}, z_{i+1}, z_i)dz_i dz_{i+1}$$

$$-\frac{1}{8\pi}\sum_{i=2}^{n_E}\int_{-\infty}^{+\infty}\int_{-\infty}^{+\infty} q_{e_i}^{-}(z_{i-1} - z_i)\nu_{i-1}V_{z_{i-1},\mathbf{r}}\frac{e^{-jkr_{\mathbf{r},z_{i-1}}}}{r_{\mathbf{r},z_{i-1}}}\frac{e^{-jkr_{z_{i-1},z_i}}}{r_{z_{i-1},z_i}}\beta_{\mathbf{r},e_{i-1},e_i}(\mathbf{r}, z_{i-1}, z_i)dz_i dz_{i-1}$$

Symmetry can be used in the same way as for the integral equation,

$$p_{\mathrm{HOD}}(\mathbf{r}) = -\frac{1}{4\pi}\sum_{i=1}^{n_E-1}\int_{0}^{+\infty}\int_{-\infty}^{+\infty} q_{e_i}^{+}(z_{i+1} - z_i)\nu_{i+1}V_{z_{i+1},\mathbf{r}}\frac{e^{-jkr_{\mathbf{r},z_{i+1}}}}{r_{\mathbf{r},z_{i+1}}}\frac{e^{-jkr_{z_{i+1},z_i}}}{r_{z_{i+1},z_i}}\left[\beta_{\mathbf{r},e_{i+1},e_i}(\mathbf{r}, z_{i+1}, z_i)\right.$$

$$\left.+\beta_{\mathbf{r},e_{i+1},e_i}(\mathbf{r}, -z_{i+1}, z_i)\right]dz_i dz_{i+1}$$

$$-\frac{1}{4\pi}\sum_{i=2}^{n_E}\int_{0}^{+\infty}\int_{-\infty}^{+\infty} q_{e_i}^{-}(z_{i-1} - z_i)\nu_{i-1}V_{z_{i-1},\mathbf{r}}\frac{e^{-jkr_{\mathbf{r},z_{i-1}}}}{r_{\mathbf{r},z_{i-1}}}\frac{e^{-jkr_{z_{i-1},z_i}}}{r_{z_{i-1},z_i}}\left[\beta_{\mathbf{r},e_{i-1},e_i}(\mathbf{r}, z_{i-1}, z_i)\right.$$

$$\left.+\beta_{\mathbf{r},e_{i-1},e_i}(\mathbf{r}, -z_{i-1}, z_i)\right]dz_i dz_{i-1} \tag{9}$$

It should be noted that the receiver could be in the near- or far-field of the noise barrier. In section 2.2, the incoming/source field was restricted to be a plane- or cylindrical wave field, which lead to the possibility to exploit the resulting symmetry and use the compact form of the edge source signals. In this propagation integral, however, no such restriction is introduced as regards receiver position, which implies that a double integral is needed.

3 COMPUTATIONAL ASPECTS

3.1 Matrix formulations

The integral equations can be solved in a straighforward way, with the Nyström method[12], which involves a discretization of the unknown functions/signals, $q^{\pm}_{e_i}(z)$. The semi-infinite range, $z \in [0, \infty]$, will have to be truncated to some value z_{max}. Then the set of N discretized values of the unknown function $q^{\pm}_{e_i}(z)$ can be written in a column vector,

$$\mathbf{q}^{\pm}_{e_i} = [q^{\pm}_{e_i}(0), q^{\pm}_{e_i}(z_1), ..., q^{\pm}_{e_i}(z_N)]^T$$

and the integral equation in Eq. (8) becomes a matrix equation

$$\mathbf{q}^{+}_{e_i} = \mathbf{q}^{+}_{e_i,0} + \mathbf{H}_{e_{i+1},e_i,e_{i-1}} \mathbf{q}^{+}_{e_{i-1}}$$

where $\mathbf{H}_{e_{i+1},e_i,e_{i-1}}$ is a full (N, N) matrix which contains the transfer function values from all N edge points along edge e_{i-1}, via $z = 0$ along edge e_i, to all N edge points along edge e_{i+1}. The set of integral equations, and corresponding set of unknowns, $\mathbf{q}^{+}_{e_1}, \mathbf{q}^{+}_{e_2}, \mathbf{q}^{-}_{e_2}, ...$, can furthermore be packed into a single matrix equation by stacking the unknowns into one large column vector, $\mathbf{q}$,

$$\mathbf{q}_{\text{open cylinder}} = \left[\mathbf{q}^{+}_{e_1}, \mathbf{q}^{+}_{e_2}, \mathbf{q}^{-}_{e_2}, ..., \mathbf{q}^{-}_{e_{N-1}}, \mathbf{q}^{-}_{e_N}\right]^T \tag{10}$$

Here we have chosen the "open cylinder" case where edge e_N can not see edge e_1, see Figure 1b, which corresponds to a noise barrier without a hard-ground reflection. On the other hand, for a polygonal cylindrical shape with finite cross-section, a "closed cylinder", Figure 1a, which results if one represents a hard ground by a mirror image of the noise barrier, then the vector of unknowns also includes $\mathbf{q}^{+}_{e_N}$ and $\mathbf{q}^{-}_{e_1}$,

$$\mathbf{q}_{\text{closed cylinder}} = \left[\mathbf{q}^{+}_{e_1}, \mathbf{q}^{-}_{e_1}, \mathbf{q}^{+}_{e_2}, \mathbf{q}^{-}_{e_2}, ..., \mathbf{q}^{+}_{e_N}, \mathbf{q}^{-}_{e_N}\right]^T \tag{11}$$

The transfer function matrices, $\mathbf{H}_{e_{i+1},e_i,e_{i-1}}$, can be correspondingly packed into one huge matrix, $\mathbf{H}$, such that

$$\mathbf{q} = \mathbf{q}_0 + \mathbf{H}\mathbf{q} \tag{12}$$

This matrix $\mathbf{H}$ will be sparse, with submatrix blocks which are full. For the open cylinder case, $\mathbf{H}$ is set up as

$$\mathbf{H} = \begin{bmatrix} \mathbf{H}_{\mathbf{q}^{+}_{e_1} \leftarrow \mathbf{q}^{+}_{e_1}} & \mathbf{H}_{\mathbf{q}^{+}_{e_1} \leftarrow \mathbf{q}^{+}_{e_2}} & \mathbf{H}_{\mathbf{q}^{+}_{e_1} \leftarrow \mathbf{q}^{-}_{e_2}} & ... \\ \mathbf{H}_{\mathbf{q}^{+}_{e_2} \leftarrow \mathbf{q}^{+}_{e_1}} & \mathbf{H}_{\mathbf{q}^{+}_{e_2} \leftarrow \mathbf{q}^{+}_{e_2}} & \mathbf{H}_{\mathbf{q}^{+}_{e_2} \leftarrow \mathbf{q}^{-}_{e_2}} & ... \\ \mathbf{H}_{\mathbf{q}^{-}_{e_2} \leftarrow \mathbf{q}^{+}_{e_1}} & \mathbf{H}_{\mathbf{q}^{-}_{e_2} \leftarrow \mathbf{q}^{+}_{e_2}} & \mathbf{H}_{\mathbf{q}^{-}_{e_2} \leftarrow \mathbf{q}^{-}_{e_2}} & ... \\ ... & ... & ... & ... \end{bmatrix}$$

where each submatrix is temporarily denoted $\mathbf{H}_{\mathbf{q}^{+}_{e_1} \leftarrow \mathbf{q}^{+}_{e_1}}$, to indicate how the submatrix represents the connection from source signal to source signal. Now, many of these submatrices will be zero, because a connection such as $\mathbf{q}^{+}_{e_1} \leftarrow \mathbf{q}^{+}_{e_1} = 0$ since $\mathbf{q}^{+}_{e_1}$ is the source signal on edge e_1, radiating in the direction of e_2. As a consequence, this source signal can not contribute again to the source signal $\mathbf{q}^{+}_{e_1}$. As a result, only one or two submatrices per row, and per column, can be non-zero, since each edge sees only one or two edges,

$$\mathbf{H} = \begin{bmatrix} 0 & 0 & \mathbf{H}_{\mathbf{q}^{+}_{e_1} \leftarrow \mathbf{q}^{-}_{e_2}} & ... \\ \mathbf{H}_{\mathbf{q}^{+}_{e_2} \leftarrow \mathbf{q}^{+}_{e_1}} & 0 & 0 & ... \\ \mathbf{H}_{\mathbf{q}^{-}_{e_2} \leftarrow \mathbf{q}^{+}_{e_1}} & 0 & 0 & ... \\ ... & ... & ... & ... \end{bmatrix} = \begin{bmatrix} 0 & 0 & \mathbf{H}_{e_2,e_1,e_2} & ... \\ \mathbf{H}_{e_3,e_2,e_1} & 0 & 0 & ... \\ \mathbf{H}_{e_1,e_2,e_1} & 0 & 0 & ... \\ ... & ... & ... & ... \end{bmatrix} \tag{13}$$

where we restored the notation $\mathbf{H}_{e_1,e_2,e_1}$ for the submatrices. One can observe that the submatrices along the diagonal will all be zero. This matrix equation can either be solved with direct inversion,

$$\mathbf{q} = [\mathbf{I} - \mathbf{H}]^{-1} \mathbf{q}_0 \tag{14}$$

or via an iterative solution,

$$\mathbf{q}_n = \mathbf{H}\mathbf{q}_{n-1} \qquad n = 1, 2, ... \tag{15}$$

where the results of any iteration step, $\mathbf{q}_n$, can be propagated to a receiver position and give exactly the diffracted sound pressure up to and including order n+2 of diffraction. The number of iteration steps needed is usually small, on the order of 10. Geometries with many small facets, which implies that diffraction waves travel across many edges, do, however, require larger numbers of iteration steps.

The solving of the integral equation, that is, solving matrix equation Eq. (12), is typically the most time-consuming stage of the solution. Once $\mathbf{q}$ has been found, the propagation double integral in Eq. (9), can be represented by another matrix equation,

$$p_{\mathrm{HOD}}(\mathbf{r}) = \mathbf{F}\mathbf{q} \tag{16}$$

where $\mathbf{F}$ contains all the integrand/transfer function values from all edge source signals in $\mathbf{q}$ to a single receiver position.

3.2 Computational challenges

Discretization

The edges are discretized when the integral equations are turned into a matrix equation formulation, which implements the Nyström method, and in the same way as surface-element, and volume-element discretization schemes, a number of elements will be needed per wavelength. Using a standard Gauss-Legendre quadrature scheme for the discretization of the edges typically leads to a need for two elements per wavelength to reach within 1% of the final value.

Singularity issues

As discussed by Asheim and Svensson[12], there are three singularity challenges that are all caused by the discontinuous nature of the β-function:

1. The source term: whenever the source is in the plane of two edges, the β-function becomes singular.

2. The transfer function matrix: whenever two adjacent polygons of the scattering polyhedron are close to co-planar, then the β-function becomes close to singular.

3. The propagation integral: when a receiver position is in the plane of two edges, the β-function becomes singular.

These singularity issues can be handled by replacing the β-function with the first term of the serial expansion, as shown by Svensson and Calamia for the first-order diffraction integral[15]. That approach leads to that for small parts of the integration ranges, the explicit β-function should be replaced by its serial expansion, which can subsequently by solved analytically. The propagation singularity can be handled by a two-stage hybrid ESIE/BEM approach. In the first stage, the ESIE method suggested here can be used to compute the pressure at a number of points along the surface of the scattering object. In the second stage, these surface pressures are then propagated to the external receiver point of interest using the propagation integral of the BE method, since the propagation stage of the BE method has no singularity issues[18].

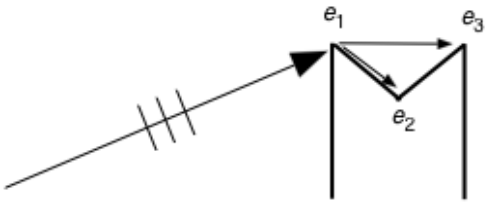

Figure 2 – A non-convex noise barrier top, with diffraction wave paths from edge e_1 indicated.

Non-convex geometries

The need to discuss separately non-convex geometries is caused by the so-called slope diffraction phenomenon. This aspect deals with the validity of the underlying formulation, and it is therefore not a numerical challenge. However, it is described here, together with other challenges for the method. The slope-diffraction phenomenon means that an edge which is hit by a wave of zero sound pressure, but a non-zero gradient in the direction which is perpendicular to the edge and to the direction of propagation, will generate a diffracted wave via "slope-diffraction": the edge is hit by a slope, or gradient. The edge-source integral equation cascades, or multiplies together, edge source amplitudes and directivity functions for consecutive edges, and this approach leads to that slope diffraction can not appear. It was shown by Summers[16] that a potential worst-case example is an opening in a thin baffle, for which the edge source integral equation leads to an error on the order of a few dB for very low frequencies. As shown by Martin and Svensson[17], it is possible to introduce complementary dipole-style edge sources, but they can be used only for high frequencies. Many scattering objects clearly have non-convex geometries, but not the worst case of a hole in a thin plate/baffle. Noise barriers with Y-shaped tops are such examples, which will be investigated among the numerical examples below. Figure 2 shows one example of such a top, and the arrows indicate one of the aspects of a non-convex geometry: edge e_1 can reach both edge e_2 and e_3. With many smaller facets, a large number of edges can see each other, but this edge-to-edge visibility is taken care of when one sets up the matrix equation to solve. A more important factor is the fact that a diffraction waves which does not travel along a rigid surface, such as the $e_1 \Rightarrow e_3$ diffraction wave in Figure 2, then smaller or larger amounts of slope diffraction is generated, and slope diffraction can not be handled by the ESIE method. Furthermore, as a recession gets deeper and deeper, specular reflection of higher and higher orders will need to be included in the edge-to-edge paths, so the computational complexity increases steadily as a geometry becomes less and less convex.

4 NUMERICAL EXAMPLES

Results will be presented below for several different noise barriers: (1) a thick noise barrier of 1m width, 40m length, infinite extension in the vertical direction, and a flat top, see Figure 3a; (2) same as case (1) but with a triangular top, see Figure 3b.

4.1 Directivity of sound field components

A first demonstration will illustrate how the four components of Eq. 1 have their visibility zones distributed around the different noise barrier geometries, and how the total sound field adds up to a continuous, smooth curve across these discontinuities. Figure 4a shows the results for the flat-top barrier in Figure 3a on a linear amplitude scale, relative to the incident plane wave amplitude. It can be observed that the first-order diffraction component compensates for the direct sound and specular reflection discontinuities, while the higher-order component varies smoothly across those discontinuities. On the other hand, the higher-order component component compensates for the first-order diffraction discontinuity around the receiver angle of 0 degrees. All in all, the total field is a smooth curve everywhere, and for receiver angles larger than around 165 degrees, interference effects between the direct sound and reflection appear, including one peak which has more than twice the amplitude of the incident plane wave, due to the first-order diffraction contribu-

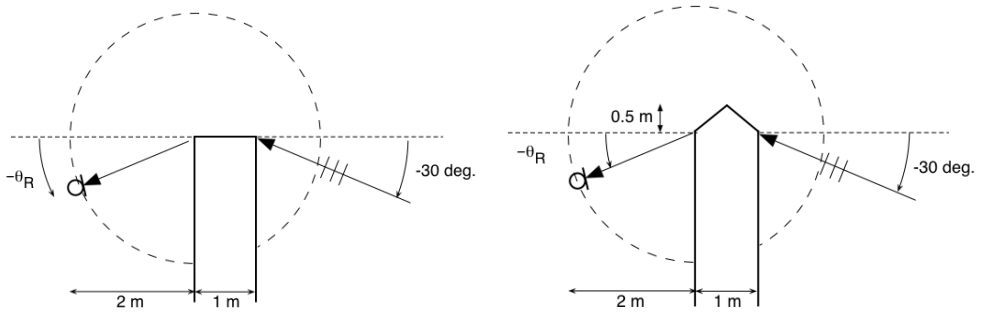

(a) (b)

Figure 3 – Geometry of two noise barriers, with (a) Flat top, (b) Triangular top.

tion. For the presented results, the 40 m long edge was discretized uniformly with 1499 elements, implying 25 elements per wavelength.

The triangular-top barrier in Figure 3b generates one narrow zone of specular reflection visibility, around 90 degrees receiver angle, that is, almost straight up above the noise barrier. Also this specular reflection discontinuity is compensated for by the first-order diffraction wave.

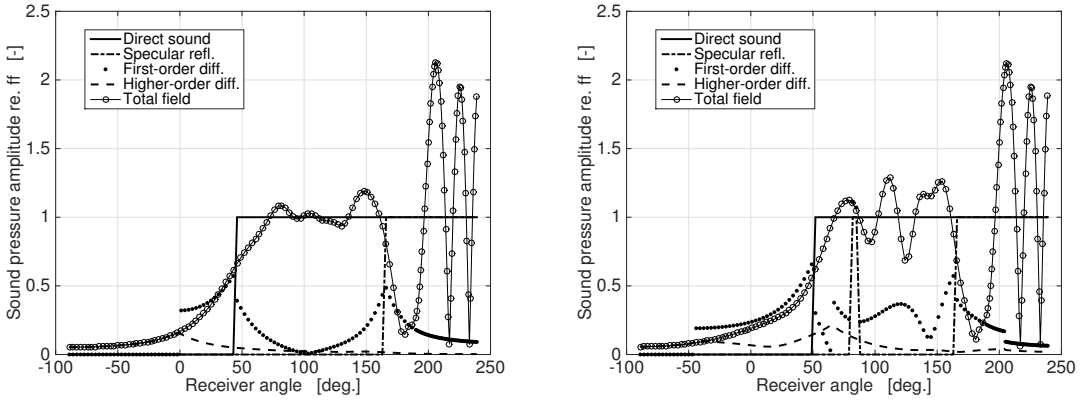

(a) (b)

Figure 4 – The distribution of sound field components, as well as the total sound field, around the two noise barrier types in Figure 3. Results for the flat-top geometry are shown in (a), while (b) shows results for the triangular-top geometry. The sound pressure amplitude is normalized against the plane wave incidence, and is shown on a linear scale.

4.2 Required discretization

A second demonstration will show how the discretization of the edge affects the accuracy of the results. A single receiver position at -45 degrees, for the flat-top noise barrier is used as test-case, with a plane-wave incidence angle of -30 degrees, see Figure 5a, or -5 degrees, see Figure 5b. A number of different discretizations were used, and the results with the highest discretization (1499 elements) were used as a reference. Based on these reference results, the relative error was computed, and is plotted against number of elements per wavelength in Figure fig:thickbarrierSresults. Several observations can be made. First, the errors in Figure fig:thickbarrierS5results are substantially higher than those in Figure fig:thickbarrierS30results for all but the finest discretization. The reason is that the source term is close to singular with the incidence angle close to the two edges forming the noise barrier top. A second aspect of this singularity is that the error is independent of number of elements per wavelength but depends on the

total number of discretization points. A third observation is that apart from the singularity challenge, the edges might need to have a minimum number of around 100 discretization points, and 2 elements per wavelength, in order to reach an error comfortably below 1%. The singularity could be handled by a serial expansion of the β-function, as used by Svensson and Calamia for first-order diffraction[15]. Finally, it should be noticed that the implementation here was rather simple, using uniform discretization, rather than Gauss-Legendre, which could be expected to converge even faster.

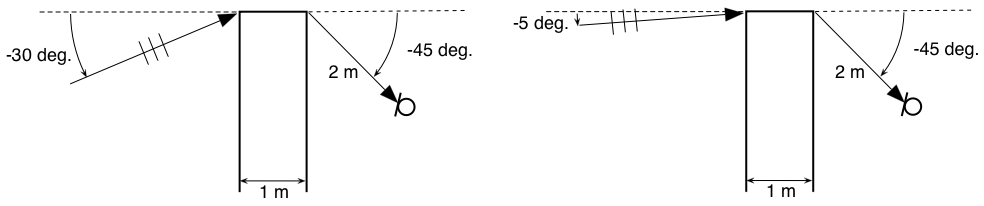

(a) (b)

Figure 5 – Geometry for a flat-top noise barrier, with plane wave incidence angles of (a) -30 degrees, and (b) -5 degrees, relative to horizontal incidence.

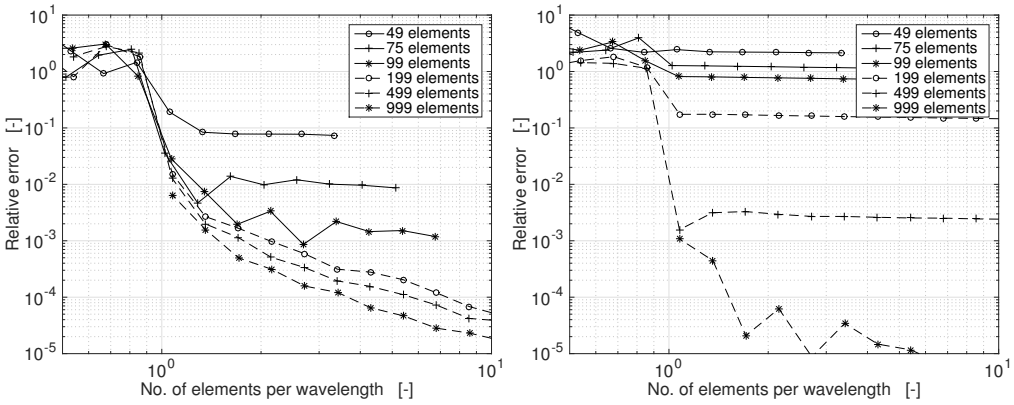

(a) (b)

Figure 6 – Relative error for the sound pressure amplitude for a flat-top noise barrier, with plane wave incidence angles of (a) -30 degrees, and (b) -5 degrees, relative to horizontal incidence, as shown in Figure 5.

4.3 Convergence for very low frequency

One of the challenges for a method which is based on geometrical acoustics is the accuracy for low frequencies. It has been shown previously that the ESIE method converges to the correct results for very low frequencies, for rigid, convex scatterers[12], whereas there is a significant error for the worst-case geometry of a hole in a thin baffle[16].

This low-frequency is investigated here by computing the response for the frequency 0 Hz, and a receiver position placed as in Figure 7, for three different noise barrier tops, including an inverted triangular shape, which creates a non-convex geometry. As a consequence, the latter geometry should introduce the slope diffraction phenomenon, which is ignored by the ESIE approach. The convergence was studied as follows. The integration range, corresponding to noise barrier length, was increased in steps of 2: 40m, 80m, 160m etc. For each length, the number of discretization points was increased until the relative change in sound pressure amplitude (for 0 Hz) was smaller than 10^{-4}. In addition, Richardson extrapolation was applied, and the computed as

well as extrapolated results are shown in Figure 8. As one example, the extrapolated result for the barrier length 160m is based on the three results: 40m, 80m, and 160m.

A first observation is that the results for the frequency 0 Hz are converging slowly, requiring very long barrier lengths. At the same time, Richardson extrapolation works remarkably well and gives stable estimates already from barrier lengths of 160m or 320m. For the two convex geometries in Figures 7a and 7b, the estimated values based on extrapolation are within 0.005 dB of the expected value of 1. Then, for the non-convex geometry in Figure 7c, a slight difference can be identified between the theoretical value 1, and the estimate based on extrapolation. This difference is around 0.04 dB, so it seems like a recessed noise barrier top as in Figure 7c cause very small amounts of slope diffraction, and the ESIE-based methods should work well.

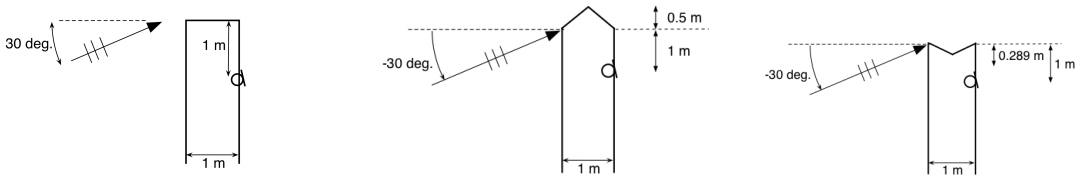

(a) (b) (c)

Figure 7 – A thick noise barrier with three different tops, with an incident plane wave as illustrated. A receiver is placed immediately at the surface of the noise barrier, as is also illustrated.

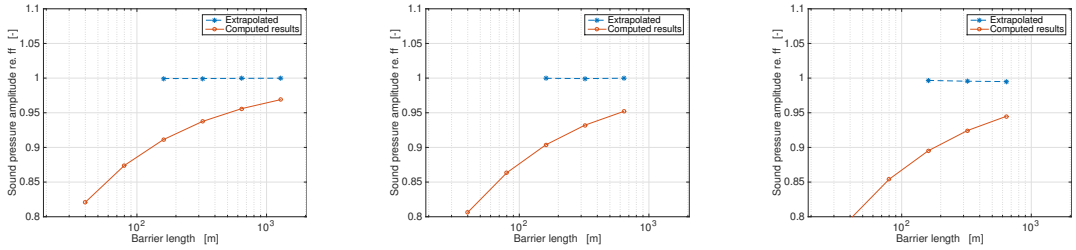

(a) (b) (c)

Figure 8 – The sound pressure amplitude, re. to the incident free-field amplitude, as function of noise barrier length, for the frequency 0 Hz. The three diagrams refer to Figures 7a,7b, and 7c, respectively. The curve denoted "Extrapolated" refer to Richardson extrapolated values, based on the computed ones.

5 CONCLUSIONS

A reformulation has been presented of the edge source integral equation for studying the insertion loss of noise barriers with parallel edges. Whereas the previous general formulation can handle arbitrary finite 3D, convex-shaped scattering objects, the formulation presented here is especially efficient for noise barriers with parallel edges only. It has been demonstrated that the method converges to correct values for very low frequencies, for rigid convex barrier shapes. For an example noise barrier top with a shallow recession - a simple type of non-convex geometry - the error for very low frequencies was smaller than 0.1 dB. The accuracy for higher frequencies is guaranteed by the method's basis in geometrical acoustics. Furthermore, it has been shown that the discretization seems to require around 100 elements per edge, and also at least two element's per wavelength, for an accuracy better than 1%. The method has some challenges for discrete external source angles, as well as radiation angles, where the involved integrals might converge very slowly. Further work is needed to handle these issues, e.g. by a reformulation of the integrand functions using a serial expansion around the singular point.

ACKNOWLEDGEMENTS

Part of this research was funded by the Norwegian Research Council, project "Hybrid method for calculating the radiated sound from vibrating structures".

6 References

1. Maekawa Z. Noise reduction by screens. Appl Ac. 1968; 1: 157–173.
2. Kurze UJ, Anderson GS. Sound attenuations by barriers. Appl Ac. 1971; 4: 35–53.
3. Hothersall DC, Chandler-Wilde SN, Hajmirzae MN. Efficiency of single noise barriers. J Sound Vib. 1991; 146: 303–322.
4. Duhamel D. Efficient calculation of the three-dimensional sound pressure field around a noise barrier. J Sound Vib. 1996; 197: 547–571.
5. Macdonald HM. A class of diffraction problems. Proc. London Math. Soc. 1915; 2: 410–427.
6. Biot MA, Tolstoy I. Formulation of wave propagation in infinite media by normal coordinates with an application to diffraction. J Acoust Soc Am. 1957; 29: 381–391.
7. Tolstoy I. Exact, explicit solutions for diffraction by hard sound barriers and seamounts. J Acoust Soc Am. 1989; 85: 661–669.
8. Kawai T. Sound diffraction by a many-sided barrier or pillar. J Sound Vib. 1981; 79: 229–242.
9. Medwin H. Shadowing by finite noise barriers. J Acoust. Soc Am. 1981; 69: 1060–1064.
10. Svensson UP, Fred RI, Vanderkooy J. An analytic secondary source model of edge diffraction impulse responses. J Acoust Soc Am. 1999;106: 2331–2344.
11. Svensson UP, Calamia PT Nakanishi S. Frequency-domain edge diffraction for finite and infinite edges. Acta Acustica/Acustica. 2009; 95: 568–572.
12. Asheim A, Svensson UP. An integral equation formulation for the diffraction from convex plates and polyhedra. J Acoust Soc Am. 2013; 133: 3681–3691.
13. Svensson UP, Asheim A. Time-domain formulation of an edge source integral equation. Proc. Meetings of Acoust. 2013; 19: 015103.
14. Asheim A, Svensson UP. Efficient evaluation of edge diffraction integrals using the numerical method of steepest descent. J Acoust Soc Am. 2010; 128: 1590–1597.
15. Svensson UP, Calamia PT. Edge-diffraction impulse responses near specular-zone and shadow-zone boundaries. Acta Acustica/Acustica. 2006; 92: 501–512.
16. Summers JE. Inaccuracy in the treatment of multiple-order diffraction by secondary-edge-source methods. J Acoust Soc Am. 2013; 133: 3673–3676.
17. Martin SR, Svensson UP. Double diffraction models: a study for the case of non-convex bodies. Proc Forum Acusticum; 7-12 September 2014; Krakow, Poland 2014.
18. Martin SRM, Svensson UP, Šlechta J, Smith J. O. A hybrid method combining the edge source integral equation and the boundary element method for scattering problems. 171st Meeting of the Acoust Soc Am.; 23-27 Ma7 2016; Salt Lake City, Utah, USA 2016.